Numerical simulation of the operation of the GPR experiment on NETLANDER

V. Ciarletti,[1] B. Martinat,[1,2] A. Reineix,[2] J. J. Berthelier,[3] and R. Ney[3]

Received 13 February 2002; revised 20 June 2002; accepted 3 July 2002; published 8 February 2003.

[1] The first objective of the Ground-Penetrating Radar (GPR) experiment on NETLANDER is to investigate the geological structures of the Martian subsurface. The aim of this paper is to present initial results obtained in the first phase of a long-term effort to build a numerical model of the GPR operation on Mars and test dedicated signal-processing algorithms on the simulated data. The simulation is based on the use of a Finite Difference Time Domain method, and we have pointed out some of its advantages that allow us to take into account complex features of the underground. This model has given reliable estimates of the power budget of the radar for a simple but still representative model of the Martian subsurface. In addition, several detailed features such as gradients and roughness at the interfaces were introduced to appraise their possible influence on the GPR performances. In the frame of a simplified geometry of both the GPR antennas and the various underground interfaces, a simple and first-order method was developed and tested on simulated data to show the ability of the GPR to retrieve a three-dimensional distribution of the underground reflectors. Based on this model, and even with some rather crude hypothesis on the subsurface electromagnetic characteristics, information on the direction and distances of the reflectors has been retrieved with a satisfactory approximation. *INDEX TERMS:* 0925 Exploration Geophysics: Magnetic and electrical methods; 0933 Exploration Geophysics: Remote sensing; 6225 Planetology: Solar System Objects: Mars; 5494 Planetology: Solid Surface Planets: Instruments and techniques; 5464 Planetology: Solid Surface Planets: Remote sensing; *KEYWORDS:* GPR, Mars, FDTD, subsurface, wave propagation, roughness

Citation: Ciarletti, V., B. Martinat, A. Reineix, J. J. Berthelier, and R. Ney, Numerical simulation of the operation of the GPR experiment on NETLANDER, *J. Geophys. Res.*, *108*(E4), 8028, doi:10.1029/2002JE001867, 2003.

1. Introduction

[2] The first objective of the Ground-Penetrating Radar (GPR) experiment on NETLANDER is to investigate the geological structures of the Martian subsurface and search for the possible existence of water reservoirs either in the form of ground ice or, at greater depths, of liquid water. The classical operation of ground-penetrating radars relies on measurements performed at a network of positions over the soil to be investigated and on the subsequent analysis of the echoes by inversion algorithms [*Habashy and Mittra*, 1987] to retrieve the three-dimensional (3-D) structure of the underground. In the case of the NETLANDER mission, the GPR will be operated from fixed landers and the instrument has been designed in an attempt to overcome this limitation and directly perform a kind of 3-D imaging of the underground reflectors. This calls for determining not only their distances but also their directions. We present in this paper some results obtained in the initial phase of a long-term effort to build a numerical model of the radar operation on Mars and test dedicated signal-processing algorithms on the simulated data. The concept of the instrument and its design approach have been described by *Berthelier et al.* [2000] and in a companion paper [*Berthelier et al.*, 2003]. Only the main characteristics are recalled here, in particular an important feature for the instrument sensitivity: since the GPR will be operated from a fixed location and aims at fixed targets, a large number of coherent integrations can be performed in order to improve the Signal/Noise ratio. *Berthelier et al.* [2000] have shown that, given the sensitivity of the electric and magnetic antennas, 2^{17} coherent additions for the electric antenna and 2^{24} for the magnetic one will overcome attenuation levels up to 185 dB.

[3] In the first paragraph, we summarize the numerical method used to model the underground wave propagation and reflection on interfaces and obstacles. We point out its advantages and in particular its adaptability when dealing with a rather complex medium with nonhorizontal and inhomogeneous layers separated by interfaces with adjustable roughness and gradients.

[4] Section 3 focuses on wave propagation and losses for a rather simple subsurface model with electromagnetic characteristics intended to represent conditions that are anticipated on Mars. Signals backscattered at various inter-

[1]Centre d'Etude des Environnements Terrestre et Planétaires/IPSL, Velizy, France.
[2]IRCOM, Université de Limoges, Limoges, France.
[3]Centre d'Etude des Environnements Terrestre et Planétaires/IPSL, Saint-Maur, France.

Copyright 2003 by the American Geophysical Union.
0148-0227/03/2002JE001867$09.00

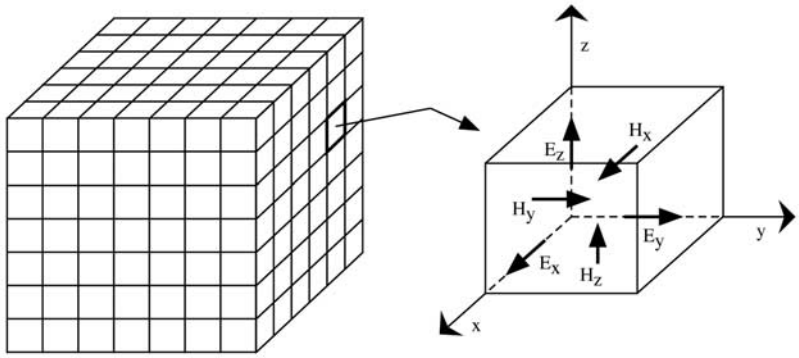

Figure 1. The computational volume and the positions where the **E** and **H** components are calculated.

faces are determined as a function of the most important parameters of the medium such as electromagnetic parameters of the soil materials and conditions at the interfaces.

[5] In section 4 we display initial results obtained during the first step of development of a method to analyze the simulated data and retrieve the position of the underground reflectors.

2. Description of the Numerical Method

[6] The ultimate objective of the work which has been undertaken is to build a numerical code that can simulate with enough accuracy the operation of the GPR in an actual environment in order to evaluate the real performances of the instrument, help preparing the signal-processing methods on simulated data and provide a tool which will be used for data inversion. Such a code must allow us to take into account the entire system, starting with the actual signals fed to the electric antenna at emission, simulating the antenna operation, the wave propagation and backscattering in the subsurface and ending by computing the electromagnetic field of waves exiting from the surface at the lander position and the corresponding current generated in the electric antennas and sent to the receiver input. We have selected the Finite Difference Time Domain (FDTD) method [*Taflove*, 1995] to describe the wave propagation and electromagnetic coupling of the antenna with the soil. Compared to methods operating in the frequency domain, which may run faster, it offers definite advantages for our problem. First it is based on a rigorous formulation and solves directly the set of Maxwell equations without any approximation. It is a versatile method quite easy to implement and the accuracy of the numerical scheme can be controlled. Working in the time domain is clearly an advantage since the exact waveform from the power amplifier is used as the input signal and subsequent propagation and backscattering of the waves can be followed in a straightforward manner. Finally, it is a three dimensional approach which allows us to represent the exact profiles and nonhomogeneities of the electromagnetic properties of the various subsurface layers down to the scale of the spatial mesh size. In addition to the derivation of a suitable electromagnetic model of the underground which is described by *Berthelier et al.* [2003] and will be briefly recalled in the next section, one of the major tasks is to build a representative model of the electric antennas, taking into account their impedance profile, their coupling with the shallow subsurface and the effects of their mutual cross coupling as well as with the lander structure. In order to properly determine the radiation pattern and the transmitted power, the simulation code describes the mutual interaction between currents and electromagnetic fields at the antenna level to derive the varying electric and magnetic field components along the antenna from which the propagation in the subsurface can be modeled. FDTD methods have been recently selected by other authors involved in the development of ground-penetrating radars for near subsurface applications [*Bourgeois and Smith*, 1997] or of airborne radars [*Demarest et al.*, 1996].

[7] The numerical algorithm, described in more detail by *Martinat* [2001] and B. Martinat and A. Reineix (manuscript in preparation, 2002), is based on the well-known work of *Yee* [1996]. It relies on the discretization and resolution of Maxwell curl equations using a time stepping procedure:

$$\begin{aligned} \mathbf{curlE}(M,t) &= -\frac{\partial \mathbf{B}}{\partial t}(M,t) \\ \mathbf{curlH}(M,t) &= -\frac{\partial \mathbf{D}}{\partial t}(M,t) + \mathbf{j}(M,t) \end{aligned} \tag{1}$$

[8] Since these equations only contain first-order space and time derivatives, the centering principle allows us to obtain a second-order accuracy: each derivative is calculated using only two field components apart from the computation point,

$$\frac{\partial f}{\partial t}(t_o) = \frac{f(t_0 + \Delta t/2) - f(t - \Delta t/2)}{\Delta t} + 0(\Delta t2) \tag{2}$$

[9] The time stepping procedure consists in solving alternatively the first and the second equation in (1) under their explicit form over the whole space domain, which is discretized by a 3-D orthogonal mesh. The basic idea of *Yee* [1996] was to define the adequate positions where each field component is calculated in order to use the centered derivatives method for the space **curl** operator approximation. These positions are indicated in the diagram of Figure 1.

[10] The FDTD method does not rely on any physical approximation, but the size of the discrete volume elements making up the computation box must be small enough to avoid numerical dispersion: it is generally admitted that the discretization step should be of the order of one tenth of a

wavelength to get reliable results. The central frequency of the GPR is 2MHz (corresponding to a 50 meters wavelength for a relative permittivity $\varepsilon_r = 9$ in the soil) and the highest frequency in the transmitted pulse bandwidth is about 5 MHz (equivalent to a wavelength of 20 meters in the same conditions). We have chosen a mesh size of 1 meter in each direction, which proved to be sufficient for propagation studies as well as to describe the underground structures with enough resolution. The time step is equal to $2\ 10^{-9}$ s for a pulse duration of 10^{-6} s.

[11] One of the major problems involved in such numerical simulations is the size of the computing box and the choice of convenient boundary conditions. These latter must allow us to properly simulate the propagation of waves in a naturally infinite medium and suppress all parasitic effects due to the spurious numerical reflection of the waves on the six external faces of the computation box. To this aim, specific electromagnetic properties are imposed to the medium at the periphery of the computing box by introducing fictitious electric and magnetic losses that theoretically suppress the reflection of waves irrespective of their angle of incidence. This method, based on the concept of "Perfectly Matched Layers" (PML), was originally developed by *Berenger* [1994] and validated for various conditions with dispersive and conductive propagation media [*Martinat et al.*, 2000; *Berenger et al.*, 2000]. A further improvement, the so-called "Convolution PML", was proposed recently by *Gedney* [1996] and has been used in the present work. Typically, for the simulations concerning an interface located at 400 meters below the antenna, the horizontal extension of the computation box has been limited to 200 meters, which has been proved to be sufficient for the studied subsurfaces.

[12] The electric antennas have been modeled as thin wires. Two additional equations have to be added to the Maxwell curl equation (1) in order to compute the currents and the charges flowing along the wires. The corresponding algorithm, developed by *Holland and Simpson* [1981], has been widely used in many areas of applications in particular for antenna design and studies in EMC. It was validated by comparison with previously developed methods such as the integral equation algorithm.

[13] The electromagnetic properties of the soil are automatically introduced in the three dimensional mesh representing the computation box by assigning the desired values of electric permittivity, magnetic permeability and electric conductivity at each cell. The electromagnetic characteristics of the medium may induce frequency dispersion in the propagating waves. In order to take this effect into account, all the electromagnetic parameters in each cell may be varied during successive time steps following algorithms based on physical models of the materials such as those proposed by Debye [*Luebbers et al.*, 1990] or Cole-Cole [*Torres et al.*, 1996]. The interfaces, which may have a complicated shape when roughness is considered, are discretized with the resolution offered by the mesh size.

[14] The complete modeling of the GPR operation requires the development of a 3-D code. However, this code requires large computer resources both in term of time and memory size. For this reason we have also made use of a 1-D version of the FDTD code whenever it allows to derive in a simple way interesting results. This 1-D version allows us to study the propagation of a plane wave in a horizontally stratified medium and already provides clues to a number of questions: reflection coefficients at the interfaces, the propagation time of reflected waves and propagation losses. Of course it cannot provide any information on the antenna gain and radiation pattern but these information, obtained from the 3-D version of the code can be combined with the results of the 1-D code to get the power budget for vertically propagating waves. A number of specific studies, in particular those performed to evaluate the power budget of the radar and its sensitivity, were thus conducted by coupling the 3-D and 1-D codes [*Reinex et al.*, 2001].

3. Simulation of Wave Propagation and Reflection in the Martian Subsurface

3.1. Electromagnetic Model of the Martian Subsurface

[15] Our model of the Martian subsurface consists in three main zones [see *Berthelier et al.*, 2003] and is shown schematically in Figure 2.

[16] A first zone, 400 meter thick, consisting of sedimentary deposits possibly mixed with lava layers from volcanic flows at least partially remodeled by impact processes. The uppermost part of this zone, above 150 meters in our model, is made of dry material with negligible water content. Deeper layers may already contain ground ice. The height of the permafrost roof has been thus taken at a depth of 150 meters, consistent with expectations for equatorial and low latitude regions.

[17] The second zone corresponds to the fractured porous megaregolith that can extend to considerable depths with the porosity decreasing with depth. This zone represents the most probable water reservoir with ice in the upper layers and possibly liquid water below some level. The depth of the liquid aquifer mainly depends on the local geothermal gradient and average surface temperature. We have taken a depth of 2500 meters still consistent with equatorial and low-latitude regions.

[18] The last zone is the solid basaltic basement either unfractured or with a vanishing porosity due to physical and chemical compaction [*Binder and Lange*, 1980; *Clifford*, 1981].

[19] In the present state of knowledge, precise values of the relative permittivity ε_r and of the conductivity σ in these various layers are of course impossible to predict. However, measurements on terrestrial analogs can offer a reasonable range of values for these two parameters. Shown in the sketch of Figure 2 are the ranges of values that we have adopted for the various layers. It was also assumed that the electric conductivity σ was constant in the frequency range where most of the energy of the transmitted pulse is contained, from about 800 kHz to 3.5 MHz as will be seen later.

[20] In all cases reported in the following, computations were performed using as an input a signal waveform corresponding to the one which has been selected for short-range soundings. This is a 2 MHz pulse of 1 μs duration modulated by a Gaussian envelope. Measurements on the laboratory mock-up of the GPR have shown that this theoretical shape is indeed very close to the actual waveform of the transmitted signal. The numerical transmitted

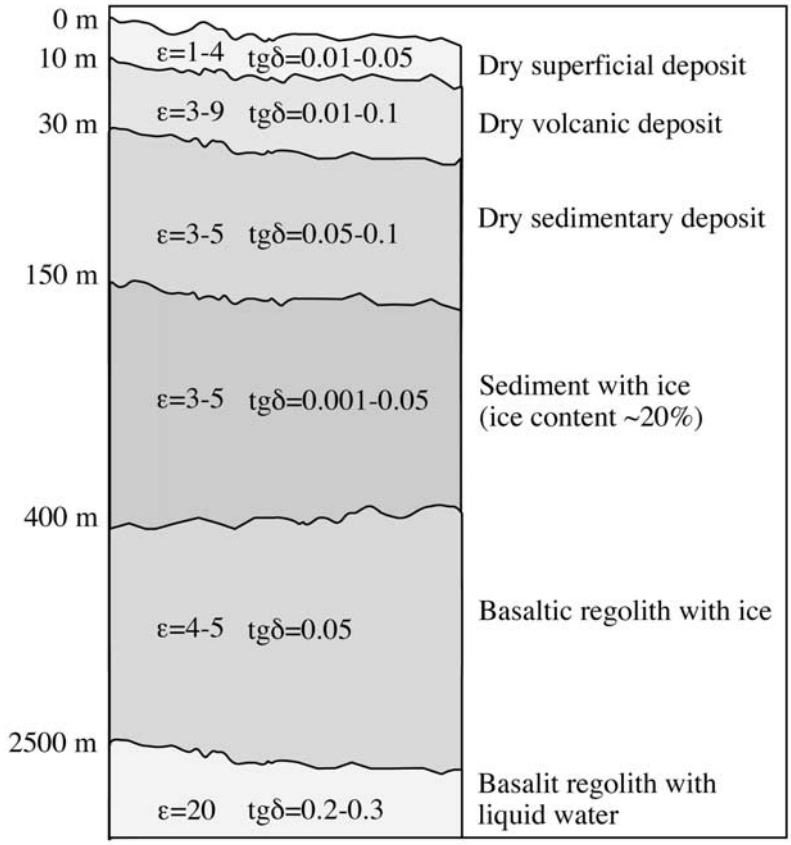

Figure 2. Martian subsurface model.

waveform and its corresponding spectrum are displayed in Figure 3a.

3.2. Propagation Losses in the Simple Case of a Plane Wave

[21] Propagation losses suffered by electromagnetic waves propagating vertically through the Martian soil and detected by the GPR after being reflected from the most interesting interfaces at 150 meters, 400 meters (upper part of the basaltic regolith partially filled with ice) and 2500 meters (depth of the liquid aquifer) were evaluated using the 1-D version of the FDTD code. These data are presented in Table 1 for the range of values of ε_r and σ which have been indicated in Figure 2. They provide an overview of the influence of the electromagnetic parameters of the medium on the attenuation of the detected waves. As instance, differences of more than 40 dB are observed for the waves reflected from the liquid aquifer between the two extreme conditions corresponding to the minimum and maximum values of ε_r and σ.

3.3. Case of Waves Transmitted With a Dipolar Antenna

[22] The first step of the numerical modeling has been conducted by considering a simplified version of the electric antennas under the form of a symmetrical dipole centered at the lander position. Due to the symmetry of a dipolar antenna, the lander structure does not play any role in the emission, and this allows us to focus this study on the sole effects brought about by the antenna radiation pattern and wave propagation in the soil and their backscattering by discontinuities either at the interfaces between various layers or by buried bodies. Computation were performed using a resistively loaded dipole as described by *Wu and King* [1965], similar to the resistively loaded monopole antennas that will be built for the GPR, which provides a wide band antenna free of the internal resonances that appear on nonloaded dipoles. In addition the dipole radiation pattern is close to the radiation pattern of a loaded monopole [*Martinat*, 2001]. The input to the simulation is the current fed to the antenna by the transmitter, the output is the current sensed by the antenna and sent to the receiver input. The evaluation of the signal attenuation and power budget of the radar is thus straightforward. An example of the results provided by the simulation runs is displayed in Figure 3, which shows the current at the receiver. The input current waveform is seen in Figure 3a together with the energy spectral density of the transmitted current. In the zoomed sections, the current at the receiver due to the reflection at the 150 meters (Figure 3b) and 400 meters (Figure 3c) interfaces are displayed together with their corresponding energy spectral density.

[23] For each echo we define a frequency dependant attenuation coefficient as the ratio between the power spectral density of the current entering the receiver and the power spectral density of the current generated by the transmitter. This attenuation coefficient includes the properties of the antenna, the spreading of the transmitted waves, their propagation losses and the coefficients of the reflections at the interfaces. It allows us to evaluate the level of

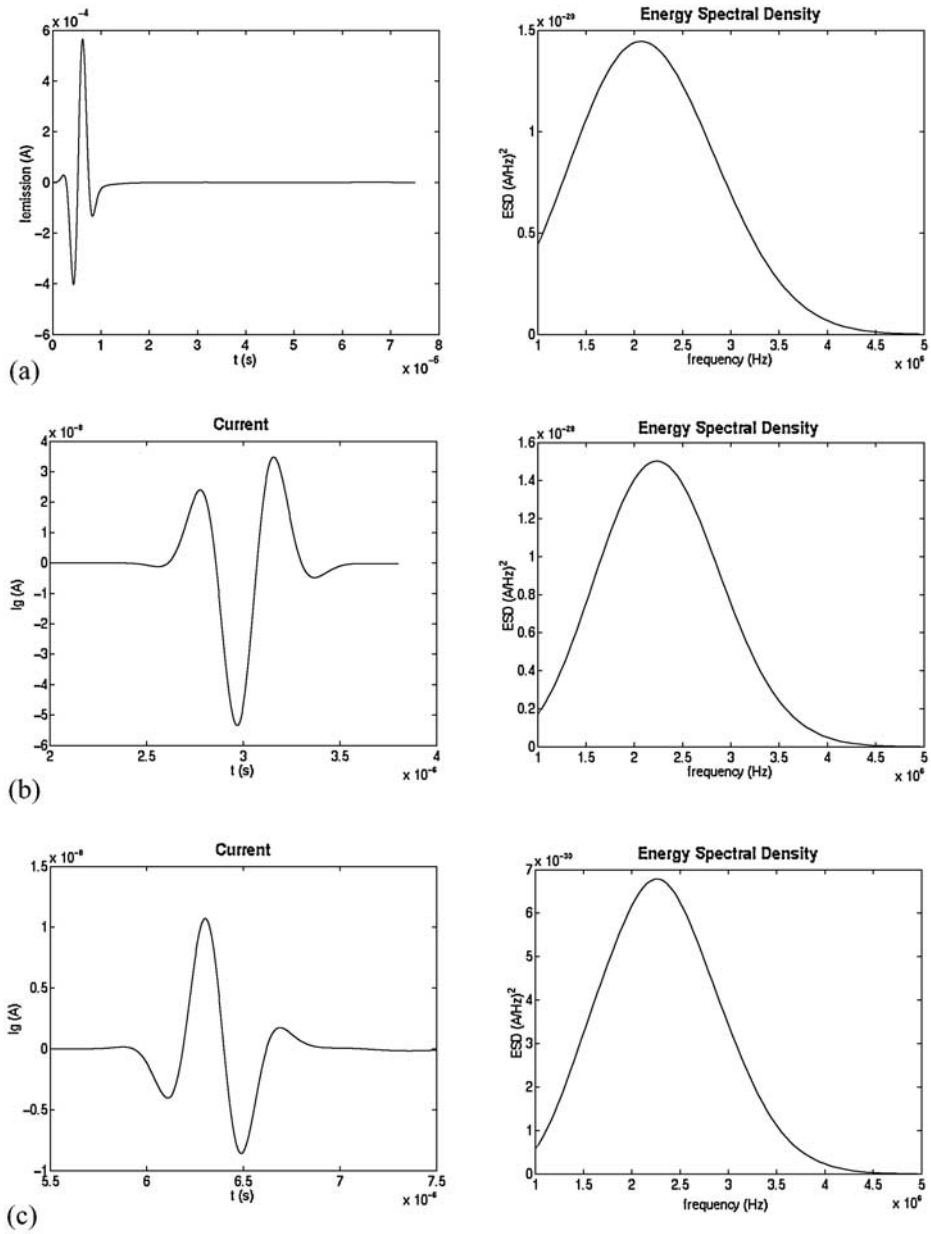

Figure 3. The current waveform at the receiver (a) and the energy spectral density corresponding to the emitted current. In the two zoomed sections (b) and (c), we show the current and energy spectral density at the receiver due to the reflection at the 150 meters (b) and 400 meters (c) interfaces.

frequency dispersion effects, which act to modify the waveform of the reflected signal. A typical result is shown in Figure 3. In most cases the attenuation coefficient does not depend significantly on frequency, and thus it can be expected that on Mars the waveform of the echoes will be similar to that of the transmitted signal. This makes somewhat simpler the development in signal processing aimed at recovering multiple echoes. From curves such as those in Figure 3, we have calculated with the 3-D version of the code the average power attenuation of the reflected signal, which is given in Table 2 for the 3 sets of values of ε_r and σ indicated in the subsurface model and for the three main interfaces.

[24] In the course of this study, we have also tried to evaluate the impact on the power budget of the radar of more realistic models of the interfaces, including roughness and continuous transitions in place of discontinuities.

[25] We have first studied the case of a diffuse reflection by introducing a rough interface at 400 meters. Since the aim of the study is to get an order of magnitude for the various phenomena of interest, we have deliberately limited ourselves to the case of a 2-D roughness imposed along the direction parallel to the dipole antenna. Future work will be dedicated to real 3-D roughness effect. The interface is therefore a cylindrical surface, which extends invariant along the axis perpendicular to the direction of the dipole

Table 1. Average Power Attenuation of the Reflected Signals for Three Main Interfaces Using the 1-D Version of the FDTD Code[a]

	Electrical Parameters (ε_r,σ)		
Depth, m	Minimum Values, dB	Mean Values, dB	Maximum Values, dB
−150	−45.9	−32.4	−35.7
−400	−27.5	−37.1	−49.1
−2500	−86.4	−108.3	−130.6

[a]The attenuation is computed using the minimum, mean, and maximum value for the permittivity and the conductivity.

antenna. An easy way to generate numerous rough and non-Gaussian surfaces is to make use of a fractal model. Since fractal description has proved to be well adapted to model the roughness of terrestrial surfaces [*Franceschetti et al.*, 1999; *Zribi et al.*, 2000] and others planetary surfaces [*Shepard and Campbell*, 1999], we can assume that it should be not too different from Martian situations. This fractal description can be obtained by many ways, among which we have selected the summation of oscillatory Weierstrass-Mandelbrot functions [*Berry and Lewis*, 1980; *Mandelbrot*, 1982]:

$$W(x) = S\sqrt{2}\frac{\sqrt{1-b(2D-4)}}{\sqrt{b(2D-4)-b(2D-4)(n2+1)}}\sum_{n=1}^{n2}\frac{1}{b(2-D)n} \cdot \cos(2\pi bnx + \theta_n) \quad (3)$$

[26] To each spatial frequency b^n, where b is an irrational number larger than 1 and n is the mode number, corresponds a random phase value θ_n and an amplitude $1/b^{(2-D)n}$. The weight of each mode depends on D, which is the fractal dimension. S is the RMS value of the altitude along the profile. Several rough profiles were generated by varying the D and S parameters respectively between 1 and 2 and between 1 to 5 meters. A typical geometry is illustrated in Figure 4.

[27] For stationary surfaces, many analytical methods based on physical assumptions (Kirchhoff, Small Perturbation Method, Integral Equation Model, etc.) [*Ogilvy*, 1991] have been developed that give the backscatter cross section as a function of the surface geometrical parameters. However, in the case of fractal surfaces, the geometrical parameters such as the RMS height variations and the correlation length increase as the surface sample area is increased and, consequently, none of these classical methods can be used. Different ways to compute statistical averages on the electromagnetic field backscattered by a fractal surface have been proposed [*Shepard*, 1999; *Franceschetti et al.*, 1999]. Our code doest not aim at providing statistical results but rather to simulate in detail the GPR operation in various representative situations and obtain simulated signals that can be used to evaluate the radar performances and develop data processing algorithms. To get some statistical estimates of the effect of rough interfaces we have run our model on a number of cases with various values of the parameters defining the fractal representation of the interfaces. Figure 5 presents three curves indicating the range of the attenuation coefficient as deduced from an analysis over 50 test interfaces with moderate roughness. Diffusive reflection over moderately rough surfaces does not result in any significant increase in the reflected signal attenuation with

Table 2. Average Power Attenuation of the Reflected Signals for Three Main Interfaces Using the 3-D Code[a]

	Electrical Parameters (ε_r,σ)		
Depth, m	Minimum Values, dB	Mean Values, dB	Maximum Values, dB
−150	−94.3	−84.2	−85.6
−400	−83.7	−94.6	−108.1
−2500	−164.0	−185.5	−208.3

[a]The attenuation is computed using the minimum, mean, and maximum value for the permittivity.

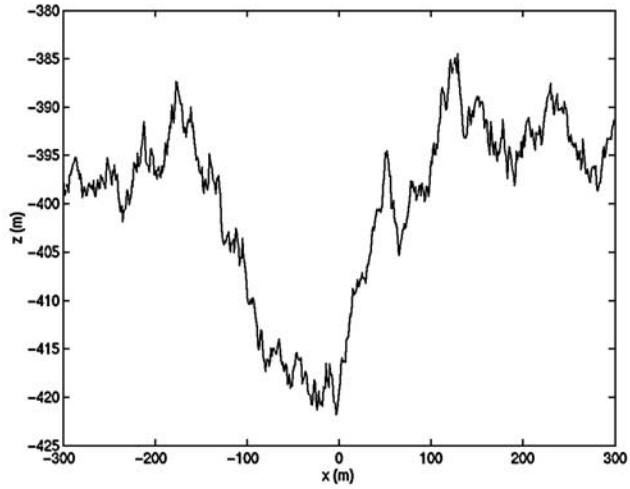

Figure 4. A typical geometry for a rough interface generated with Weierstrass-Mandelbrot function (D = 1.5, S = 2m).

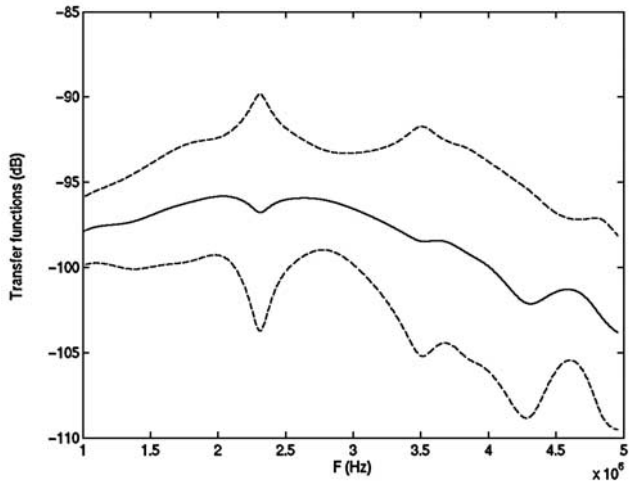

Figure 5. Influence of roughness of the −400 m interface on the transfer function. The solid curve represents the average value computed on a set of 50 rough interfaces; the two dotted curves show the standard deviation on both sides.

Table 3. Effect of a Permittivity Gradient on the Attenuation Coefficient for Two Interfaces

	Attenuation Coefficient, dB	
	−150 m Interface	−400 m Interface
No gradient	−81.16	−94.61
6 m gradient	−82.41	−95.71
10 m gradient	−84.98	−98.12
20 m gradient	−94.34	−106.01

typical values ranging from less than 2 dB at low frequencies to about 4 dB at the high frequency end of the bandwidth. The case of a very rough interface is presented in section 4.

[28] The second question, which was investigated, is the influence of magnetic materials in the uppermost layers of the soil. Investigations of the mineralogy of Martian materials conducted on direct in situ measurements by the Viking XRF [*Hargraves et al.*, 1977] or the Mars Pathfinder APXS [*Rieder et al.*, 1997] experiments, and also from remote orbital observations, have shown that the upper layers of the Martian soil is commonly constituted of weather basaltic material including a few percent of magnetic materials such as hematite or maghemite. It is therefore likely that, under such conditions, propagation losses will be increased, as was indeed observed recently on high frequency GPR measurements in the Djibouti area by *Paillou et al.* [2001]. Values of the real and imaginary components of the magnetic permeability of terrestrial materials have been published recently by *Olhoeft* [1998] for frequencies well above that of the GPR. Extrapolating these data to the 2 MHz frequency of the GPR, we have taken the following estimates for the magnetic parameters: $\mu' = 1.4$ and $\mathrm{tg}(\delta\mu) = 0.63$. Additional losses suffered by electromagnetic waves propagating through such magnetic materials were calculated in two cases, the first one with only the first superficial layer of our model, down to 10 meters, taken as "magnetic", the second one also including the second superficial layer, down to 30 meters. These additional losses amount to 3.5 dB and 15 dB respectively and a supplementary delay is observed on the returning signal due to the real part of the magnetic permeability.

[29] Finally, we have investigated an effect of more concern, which is due to the smooth transitions between two adjacent layers. Of course, smooth transitions are likely to occur more often than very sharp gradients particularly in porous rocks and in the vicinity of the freezing temperature of water: liquid water can remain mixed with solid ice over a significant height. We have thus modified the model at the 150 and 400 meters interfaces by introducing gradients in ε_r and σ over respective lengths of 6, 10 and 20 meters. Results are displayed in Table 3, which shows that such gradients induce rather significant increases in the attenuation coefficient of up to 15 dB for the smoothest transition. In this case, reflections occur within the zone of transition from an interface to the following one resulting in destructive interferences.

[30] From these set of simulations we have estimated that 15 to 20 dB should be a typical range of uncertainty on the power budgets that can be deduced from the simple layered electromagnetic model presented in the beginning of this paper. We have also started to estimate the effects of buried rocks. Although it is difficult to build any representative model since nothing is known on the rock and boulder distribution in the Martian subsurface, results obtained for the extreme case of rocks with large dimensions and with sharp differences in electric permittivity seem to preclude any large additional attenuation.

4. Retrieving the Directions of Underground Reflectors

[31] We present in this section some results obtained during the development of signal-processing methods to retrieve the direction of propagation of reflected waves. All simulated data used in this section were derived using the 3-D FDTD code described in section 2. However, for the sake of simplicity, we have considered the case of a lander with two opposite monopoles antennas with the right monopole aligned with the +X axis and the left electric monopole along the −X axis. As shown by *Berthelier et al.* [2003], the right monopole illuminates preferentially the half-space extending in the direction of the +X axis. In addition, the interfaces are modeled as surfaces extending invariant parallel to the *Y* axis. In such a geometry, waves reflected to the lander must propagate in the vertical plane of symmetry containing the X and Z (vertical) axis. The computed horizontal electric field $\mathbf{E_h}$ is, as expected from symmetry considerations, along the *X* axis and the magnetic field **H** is along the *Y* axis (see Figure 6). Simulations of course provide horizontal and vertical of **E** and **H** but, in the following calculations, we also performed the calculations of the direction of wave propagation by using only the horizontal electric component. This reproduces the real situation of the GPR, which only measures electric components in the horizontal plane.

[32] As mentioned in the previous section, due to the small enough value of the conductivity, frequency dispersion within the ~4 MHz bandwidth of the GPR is a minor effect. The waveform of the current fed to the receiver can therefore be considered similar to that of the transmitted signal. In addition, the analysis of simulated data such as those shown in Figure 3 allows us to consider the reflected electromagnetic field as the sum of several locally plane waves. The problem of retrieving the direction of propagation of reflected waves is therefore equivalent to determining the amplitude, time delay and angle of wave normal of a number of elementary waves all with the same waveform identical to the transmitted signal.

[33] Considering the jth wave and assuming that its direction of propagation is at an angle θ_j with the *z* axis, we get

$$\begin{aligned} \mathbf{E_j} &= A_j f\left(t-\tau_j\right)\left[\cos\left(\theta_j\right)\mathbf{X} + \sin\left(\theta_j\right)\mathbf{Z}\right] \\ \mathbf{H_j} &= \eta A_j f\left(t-\tau_j\right)\mathbf{Y} \end{aligned} \tag{4}$$

where $f(t)$ is the shape of the transmitted pulse A_j, is the attenuation coefficient of the reflected wave as defined in the previous section, τ_j is the propagation delay depending on the distance to the reflector and the refractive index of medium, η is the impedance of the medium.

[34] The first step of the calculation is a trial and error method to find the number of waves *N* and the optimal values of the parameters which minimize the sum of the

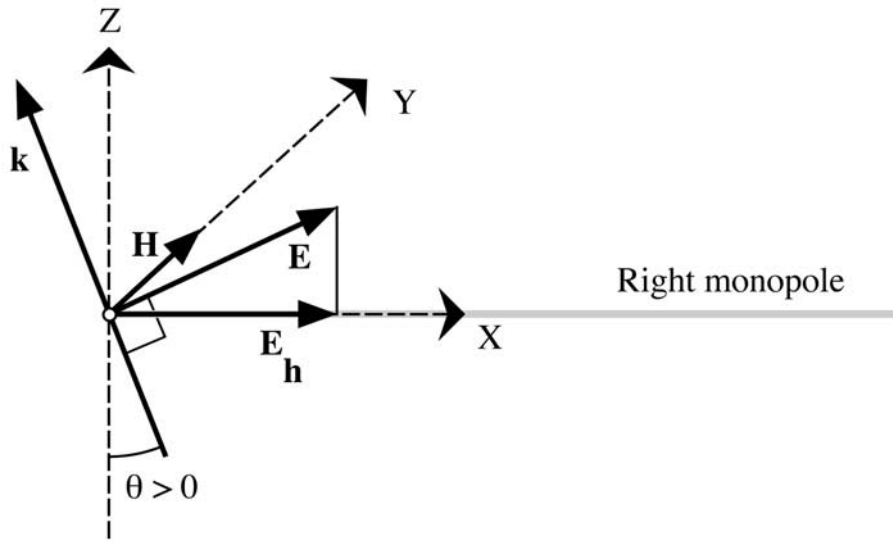

Figure 6. **E** and **H** vectors of a locally plane reflected wave for a subsurface model invariant parallel to the *Y* axis. The right monopole displayed is along +X axis.

square of the differences between the measured electric and magnetic components and their estimated values. When only the horizontal component $\mathbf{E_h}$ is available, this method only provides the cosine of the angles θ_j and therefore there is an ambiguity in the direction of the reflector. This ambiguity can be resolved by comparing the amplitudes of the two echoes obtained respectively with the right and left monopoles. For reflectors located on the +X side of the subsurface, thus corresponding to θ_j positive, the amplitude of the echo obtained when operating the right monopole is greater than when operating the left monopole. The criterion to choose the number *N* of waves is to consider only significant waves whose amplitude exceeds some threshold. In the present study we took a threshold of 10% of the major wave amplitude, but this can be easily modified.

[35] The second step is to get the information on the subsurface itself, such as the position and distance of the reflectors in the underground. With ground-penetrating radars that can be moved over the surface, echoes from a reflector detected at various positions can be used to derive an integrated value of the soil electric permittivity between the surface and the reflector. This is not possible with the GPR on a fixed lander. However, as indicated by *Berthelier et al.* [2003], the GPR includes a permittivity probe to measure the electric permittivity of the superficial layers of the soil. This allows us to deduce the angle of propagation

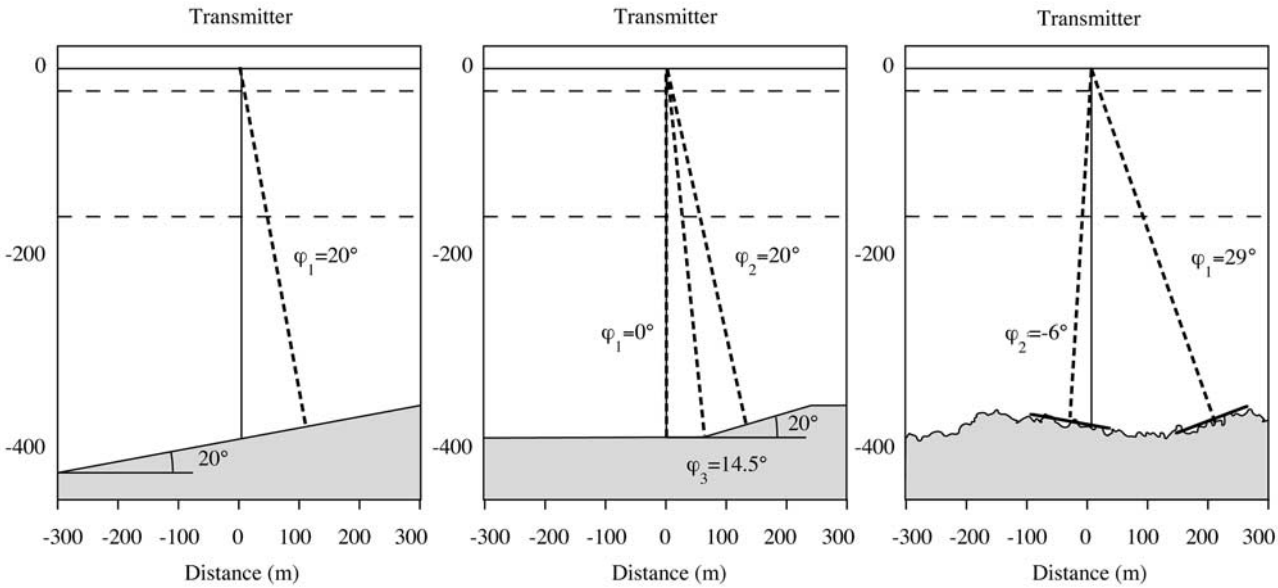

Figure 7. Three different shapes for the interface located at −400m level: a smooth inclined plane at 20° (a), a smooth horizontal plane with an inclined portion at 20° (b), and a rough interface (c).

Table 4. Computed Parameters for a Smooth Surface Inclined at 20° and Situated 400 m Below the Transmitter

		Using Ez Component		Without Ez component	
	Retrieved Parameters	Left Monopole	Right Monopole	Left Monopole	Right Monopole
Wave 1	θ_1 (°)	40.1°	37.2°	37.2°	35.8°
	τ_1 (μs)	5.94	5.91	5.94	5.91
	A_1	1.1 10^{-7}	4.9 10^{-7}	1.1 10^{-7}	4.7 10^{-7}
Reflector 1	φ_1(°)	16.7–218°	15.7–20.5°	15.7–20.5°	15.2–20.0°
	D_1(m)	326–454m	324–451m	356–454m	324–441m

of the reflected wave before it exits from the surface. Obviously, if the reflecting structure is horizontal, the backscattered wave propagates vertically in the soil and is not refracted at the interface soil/air. In this case, no assumption is needed and the direction of propagation of the reflected wave is perfectly known. In addition, we can note that all estimates of the relative electric permittivity ε_r of expected materials at some depth and above the aquifer are within a range of 3 to 6. This leads us to use a simplified approach to estimate the distance of the reflectors by taking a uniform value of the electric permittivity for the medium above the reflecting interface. We have calculated two estimates for the distance of the reflector; the first one is obtained using the maximum permittivity value and the second one using the minimum value.

[36] Focusing on the case of the interface at 400 meters, we carried out simulations to get simulated data for three different configurations of this interface that are shown in Figure 7. In each case we have indicated the likely specular reflections.

[37] For each of these configurations, we have displayed in the following tables the characteristics of the detected waves (amplitude, delay and direction of propagation above the surface) and the adjusted parameters of the reflectors deduced by the above mentioned algorithm.

[38] We are aware that calibration errors on the electric and magnetic antennas will bias the results, mainly the retrieved direction of propagation. The magnetic antenna can be perfectly calibrated using Hemotz coils and the calibration accuracy will be better than ±2% [see, e.g., *Cornilleau-Wehrlin et al.*, 1997]. Calibrating the electric antennas is much more complicated owing to their very large dimensions and the need to have no parasitic effect from the surrounding. It can only be achieved during field tests by comparison with the response of a calibrated receiver with a short dipolar antenna. An accuracy in the range of ±10% appears achievable. A sensitivity analysis has been carried out by simulation to determine the effect of these calibration errors on the estimated propagation direction. The induced errors are still within an acceptable range: for example, considering a wave propagating toward the receiving antenna with an angle of 15°, the assumed calibration errors on the electric antenna will result in an error of ±3.2° while the inaccuracy in the calibration of the magnetic antennas should lead to an error smaller than ±1° on the direction of propagation.

4.1. Case of a Smooth, Inclined Interface

[39] Results corresponding to Figure 7a are shown in Table 4. The first two columns display results obtained using horizontal and vertical components of **E** and **H** and separately for the two monopoles. They clearly show that both antennas receive the same single wave. As expected, its amplitude *A* is different from one monopole to the other one: the ratio between the amplitude received by the right monopole and the one received by the left monopole is approximately 4.5. Consequently the directivity of the radiation pattern implies a positive value for θ. The estimated angle φ in the soil ranges thus between 16° and 22°, which is in a good agreement with the 20° slope of the interface. The estimated distance lies between 330m and 454m for an expected value of 376m. This straightforward inversion of the simulated signals shows that the assumptions made on the returning waves are within acceptable limits in this simple case. Moreover, although the proposed method does not take into account the first thin layers of the subsurface model, the results are satisfactory. This indicates that these first layers do not have a major impact on the delay and direction of the returning waves.

Table 5. Computed Parameters for the Interface Presented in Figure 7b

		Using Ez Component		Without Ez Component	
	Retrieved Parameters	Left Monopole	Right Monopole	Left Monopole	Right Monopole
Wave 1	θ_1 (°)	2.8°	1.1°	2.9°	0
	τ_1 (μs)	6.24	6.23	6.24	6.23
	A_1	1.2 10^{-7}	1.4 10^{-7}	1.5 10^{-7}	1.5 10^{-7}
Reflector 1	φ_1(°)	1.2°/1.6°	0.25/0.3°	1.3/1.7°	0°
	D_1(m)	379/489m	378/488m	380/491 m	379/489 m
Wave 2	θ_2 (°)	43°	47.3°	48°	48.7°
	τ_2 (μs)	6.35	6.40	6.35	6.40
	A_2	0.5 10^{-7}	2.2 10^{-7}	0.6 10^{-7}	2.4 10^{-7}
Reflector 2	φ_2(°)	17.7/22.3°	19.2°/25.1°	19.4/25.4°	19.6/25.7°
	D_2(m)	386/498m	389/502m	386/498 m	390/503m
Wave 3	θ_3 (°)	31.5°	29.8°	32.9°	29.5°
	τ_3 (μs)	6.57	6.48	6.56	6.48
	A_3	0.15 10^{-7}	2.2 10^{-7}	0.13 10^{-7}	2.4 10^{-7}
Reflector 3	φ_3(°)	13.5°/17.6°	12.8°/16.7°	14.1°/18.3°	12.7°/16.5°
	D_3(m)	401/517m	395/509m	400/516m	395/509m

Table 6. Computed Parameters for the Rough Interface of Figure 7c

		Using Ez Component		Without Ez Component	
	Retrieved Parameters	Left Monopole	Right Monopole	Left Monopole	Right Monopole
Wave 1	θ_1 (°)	93°	73°	85.9°	59°
	τ_1 (μs)	6.56	6.51	6.74	6.50
	A_1	$2.6\ 10^{-8}$	$7.6\ 10^{-8}$	$2.6\ 10^{-8}$	$7.6\ 10^{-8}$
Reflector 1	φ_1(°)	26.5°/35.2°	25.3°/33.5°	26.5°/35.2°	25.9°/34.3°
	D_1(m)	400/516m	394/511m	412/531m	394/511m
Wave 2	θ_2 (°)	−20°	−14°	−25°	−18°
	τ_2 (μs)	5.89	5.89	5.89	5.89
	A_2	$2.5\ 10^{-7}$	$1.9\ 10^{-7}$	$2.6\ 10^{-7}$	$1.9\ 10^{-7}$
Reflector 2	φ_2(°)	−8.8/−11.4°	−6.3/−8.2°	−11.1/−14.5°	−8.2/−10.6°
	D_2(m)	355/458m	355/458m	355/458m	355/458m

[40] In the last two columns of the table, the same parameters are calculated without using the vertical component of the electric field (i.e. in the actual GPR configuration). The retrieved values show no noticeable difference with those obtained using the vertical component of **E**.

4.2. Case of an Interface With an Inclined Step

[41] In this section, the studied interface shows an inclined portion at 20° between two horizontal planes. The results are summed up in Table 5. Wave #1 corresponds to a reflection on the horizontal section. Its amplitude is roughly the same on both monopoles and the estimated distance is in agreement with the true value of 400 meters. Wave #2 comes from the inclined portion of the interface and the ratio between amplitude on the right monopole and the one on the left monopole is 4.4, consistent with the value obtained for the same angle in the previous section. As far as wave #3 is concerned, only the right monopole shows significant amplitude. Its direction of arrival is approximately 15° corresponding possibly to a wave diffracted by the edge between the horizontal and inclined parts of the interface. Results obtained with the horizontal component of the electric field only are very similar to the values retrieved using all the components. Retrieved distances for the different waves are very satisfactory.

4.3. Case of a Rough Interface

[42] The same calculations were performed in the case of a very rough interface located at an average depth of about 400m. The analysis (see Table 6) shows that the signal is composed of two main waves whose direction of propagation can be deduced from a comparison of the signals detected by the two monopoles. These directions of arrival as well as the corresponding reflector distances are in a good agreement with the geometry of the interface. A more detailed investigation shows that other weaker waves could be added to get a better fit on the simulated data but do not modify the basic result i.e. the existence of two parts of the interface acting as good reflectors.

5. Conclusion

[43] The aim of this paper was to present initial results obtained in the course of a long-term effort in numerical simulation, which has been undertaken to study the operation of the GPR experiment on NETLANDER. This simulation is based on a Finite Difference Time Domain method and we have pointed out some of its advantages. It allows us to easily take into account complex features of the underground as well as the detailed characteristics of the GPR transmitted signals. The model, which is only in a first stage of development, has already allowed us to get reliable estimates of the power budget of the radar using a simple but still representative electromagnetic model of the subsurface, which was built in accordance with the present knowledge of the geology and hydrology of Mars. In addition, several detailed features such as gradients and roughness at the interfaces were introduced to appraise their possible influence on the GPR performances. Total additional losses are estimated to be less than about 10 to 20 dB, thus within the range of the uncertainties in the estimate of the overall power budget of the radar.

[44] We have also presented initial results obtained in the domain of signal processing. In the frame of a simplified geometry of both the GPR antennas and the various underground interfaces, a simple and first-order method was developed and tested on simulated data to show the ability of the GPR to get a 3-D distribution of the underground reflectors. To provide working example, three test cases were considered which encompass situations that are likely to occur in terrestrial or Martian subsurfaces such as inclined or rough interfaces. The simulated data show that returning echoes can be considered as a sum of locally plane waves. Based on this model, and even with some rather crude hypothesis on the subsurface electromagnetic characteristics, information on the direction and distances of the reflectors have been retrieved with a satisfactory approximation.

[45] Work is in progress to extend the reported studies to more realistic and detailed descriptions of the actual 3-D geometry of both the subsurface structure and GPR antennas. Similarly, the analysis of data from field tests that are foreseen in the near future is an essential step in improving both the capabilities of the simulation code and the development of more refined signal-processing methods.

[46] **Acknowledgments.** The present work has been undertaken under the auspices of CNES grants 793/CNES/99/7947 and 737/CNES/00/8261.

References

Berenger, J. P., A perfectly matched layer for the absorption of electromagnetic waves, *J. Comput. Phys*, *114*, 185–200, 1994.

Berenger, J. P., B. Martinat, and A. Reineix A., Reflection from PMLs in lossy media, URSI Session 105, vol. 3, p. 397, Union Radio Sci. Int., Salt Lake City, 16–20 July 2000.

Berry, M. V., and Z. V. Lewis, On the Weierstrass-Mandelbrot fractal function, *Proc. R. Soc. London, Ser. A*, *370*, 459–484, 1980.

Berthelier, J. J., et al., The GPR on Netlander, *Planet. Space Sci.*, *48*(12–14), 1161–1180, 2000.

Berthelier, J. J., et al., GPR: A ground-penetrating radar for the NETLANDER mission, *J. Geophys.*, *108*, doi:10.1029/2002JE001866, in press, 2003.

Binder, A. B., and M. A. Lange, Of the thermal history of a moon of fission origin, *J. Geophys. Res.*, *85*, 3194–3208, 1980.

Bourgeois, J. M., and G. S. Smith, A complete electromagnetic simulation of a ground penetrating radar for mine detection: Theory and experiment, paper presented at *IEEE Antennas and Propagation*, Inst. of Electr. and Electron. Eng., Montreal, Canada, 1997.

Clifford, S. M., A pore volume estimate of the Martian megaregolith based on a lunar analog, in *Third International Colloquium on Mars*, *LPI Contrib. 441*, pp. 46–48, Lunar and Planet. Inst., Houston, Tex., 1981.

Cornilleau-Wehrlin, N., et al., The CLUSTER Spatio-Temporal Analysis of Field Fluctuations (STAFF) Experiment, *Space Sci. Rev.*, *79*, 107–136, 1997.

Demarest, K., Z. Huang, and R. Plumb, FDTD modeling of scatterers in stratified media, *IEEE Trans. Antennas Propag.*, *43*, 1164–1168, 1995.

Demarest, K., Z. Huang, and R. Plumb, FDTD near to far zone transformation for scatterers buried in stratified grounds, *IEEE Trans. Antennas Propag.*, *44*, 1150–1157, 1996.

Franceschetti, G., A. Iodice, M. Migliaccio, and D. Riccio, Scattering from natural rough surfaces modeled by fractional Brownian motion two-dimensional processes, *IEEE Trans. Antennas Propag.*, *47*, 1405–1415, 1999.

Gedney, S. D., An anisotropic PML absorbing media for the FDTD simulation field in lossy and dispersive media, *Electromagnetics*, *16*, 399–415, 1996.

Habashy, T. M., and R. Mittra, On some inverse methods in electromagnetics, *J. Electromagn. Waves Appl.*, *1*(1), 25–58, 1987.

Hargraves, R. B., D. W. Collinson, R. E. Arvidson, and C. R. Spitzer, The Viking magnetic properties experiments: primary mission results, *J. Geophys. Res.*, *82*, 4547–4558, 1977.

Holland, R., and L. Simpson, Finite-difference analysis EMP coupling to thin struts and wires, *IEEE Trans. Electromagn. Compat.*, *EMC-23*(2), 88–97, 1981.

Luebbers, R. J., F. Hunsberger, K. S. Kunz, and M. Schneider, A frequency dependent finite difference time domain formalism for dispersive media, *IEEE Trans. Electromagn. Compat.*, *32*, 222–227, 1990.

Mandelbrot, B. B., *The Fractal Geometry of Nature*, W.H. Freeman, New York, 1982.

Martinat, B., Etude électromagnétique du GPR de NETLANDER destiné au sondage du sous-sol martien, Ph.D. thesis, Univ. de Limoges, Limoges, France, Sept. 2001.

Martinat, B., J. P. Berenger, and A. Reinex, PML for simulation of conductive medium in FDTD, EMC Europe 2000, paper presented at 4th European Symposium on Electromagnetic Compatibility, Inst. of Electr. and Electron. Eng., Bruges, Belgium, 11–15 Sept. 2000.

Ogilvy, J. A., *Theory of Wave Scattering From Random Rough Surfaces*, Inst. of Phys., Philadelphia, Pa., 1991.

Olhoeft, G. R., Electrical, magnetic and geometric properties that determine ground penetrating radar performance, Proceedings of the 7th International Conference on Ground Penetrating Radar, Univ. of Kansas, Lawrence, 27–30 May 1998.

Paillou, P., G. Grandjean, J.-M. Malézieux, G. Ruffié, E. Heggy, D. Piponnier, P. Dubois, and J. Achache, Performances of ground penetrating radars in arid volcanic regions: Consequences for Mars subsurface exploration, *Geophys. Res. Lett.*, *28*(5), 911–914, 2001.

Reinex, A., B. Martinat, J. J. Berthelier, R. Ney, and V. Ciarletti, FDTD method of the theoretical analysis of the Netlander GPR, Poster presented at Conference on the Geophysical Detection of Subsurface Water on Mars, Lunar and Planet. Inst., Houston, Tex., 6–10 Aug. 2001.

Rieder, R., T. Economou, H. Wänke, A. Turkevitch, J. Crisp, J. Brückner, G. Dreibus, and H. Y. McSween Jr., The chemical composition of Martian soil and rocks returned by the mobile alpha proton X-ray spectrometer: Preliminary results from the X-ray mode, *Science*, *278*, 1771–1774, 1997.

Shepard, M. K., and B. A. Campbell, Radar scattering from a self-affine fractal surface: Near-nadir regime, *Icarus*, *141*, 156–171, 1999.

Taflove, A., *Computational Electrodynamics: The Finite Difference Time Domain Method*, Artech House, Norwell, Mass., 1995.

Torres, F., P. Vaudon, and B. Jecko, Application of the fractional derivatives to the FDTD modeling of pulse propagation in a cole-cole dispersive medium, *Microwave Opt. Technol. Lett.*, *15*, 300–304, 1996.

Wu, T. T., and R. W. P. King, The cylindrical antenna with non-reflecting resistive loading, *IEEE Trans. Antennas Propag.*, *AP-13*(3), 369–373, 1965.

Yee, K. S., Numerical solution of initial boundary value problems involving Maxwell's equations in isotropic media, *IEEE Trans. Antennas Propag.*, *AP-14*(4), 302–307, 1996.

Zribi, M., V. Ciarletti, and O. Taconet, Validation of a rough surface model based on fractional Brownian geometry with SIRC and ERASME radar data over Orgeval site, *Remote Sens. Environ.*, *73*, 65–72, 2000.

J. J. Berthelier and R. Ney, CETP/IPSL, 4 Avenue de Neptune, 94100 Saint-Maur, France.

V. Ciarletti and B. Martinat, CETP/IPSL, 10/12 Avenue de l'Europe, 78140 Velizy, France. (ciarletti@cetp.ipsl.fr)

A. Reineix, IRCOM, Université de Limoges, 123 Avenue Albert Thomas, 87060 Limoges Cedex, France.